In press for the Journal of Wind Engineering & Industrial Aerodynamics

CFD simulation of snow transport over flat, uniformly rough, open terrain: impact of physical and computational parameters

Luyang Kang [a], Xuanyi Zhou [a*], Twan van Hooff [b,c], Bert Blocken [b,c], Ming Gu [a]

[a] State Key Laboratory of Disaster Reduction in Civil Engineering, Tongji University, 200092 Shanghai, China
[b] Building Physics Section, Department of Civil Engineering, KU Leuven, Kasteelpark Arenberg 40 - bus 2447, 3001 Leuven, Belgium
[c] Building Physics and Services, Department of the Built Environment, Eindhoven University of Technology, P.O. box 513, 5600 MB Eindhoven, The Netherlands

Abstract

In the past, Computational fluid dynamics (CFD) simulations have been successfully applied for the prediction of snow drift around buildings and on building roofs. A literature study indicates that a wide range of influential computational and physical parameters exist for snow drifting predictions in CFD, while the impact of these parameters is unclear, resulting in a lack of available CFD simulation guidelines. Therefore, this study presents a systematic and generic analysis with emphasis on the fundamentals of snow transport prediction techniques. Snow transport over flat, uniformly rough, open terrain, including snow saltation and snow suspension is successfully simulated using CFD and the results are compared to field measurements of snow concentrations for validation. This paper investigates the impact of grid resolution, falling velocity of snow, turbulent Schmidt number, threshold friction velocity of snow and turbulence model on the CFD simulation results. The results show that the falling velocity and the turbulent Schmidt number have largest impact. A slight change in the falling velocity or the turbulent Schmidt number significantly impacts the predicted snow concentration in the air. In addition, the turbulence model mainly affect the turbulent kinetic energy, another key factor that influences the numerical predictions of snow transport.

Keywords

Snow transport; open terrain; computational fluid dynamics (CFD); sensitivity study; parametric study.

1. Introduction

In snowy and windy regions, wind-induced snow drifting can cause many problems, such as unbalanced snow loads on roofs (e.g. Irwin et al., 1995; O'Rourke et al., 2005; Thiis and O'Rourke, 2015), snowdrift around buildings (e.g. Zallen, 1988; Thiis and Gjessing, 1999), low visibility (e.g. Matsuzawa et al., 2005; Huang et al., 2008) and decreased road/railway safety (e.g. Naaim-Bouvet et al., 2002; Tabler, 2003; Liu et al., 2016). In addition to field measurements (e.g. Smedley et al., 1993; O'Rourke and Auren, 1997; Thiis and Gjessing, 1999; Tsuchiya et al., 2002; Beyers and Harms, 2003; Thiis and O'Rourke, 2015) and wind-tunnel tests (e.g. Kind, 1986; Isyumov and Mikitiuk, 1990; O'Rourke et al., 2004; Zhou et al., 2014, 2016a, 2016b), computational fluid dynamics (CFD) can be a powerful tool in solving snow-drifting engineering problems, such as the evaluation of snowdrift around buildings/structures or on building roofs (e.g. Sato et al., 1993;

Naaim et al., 1998; Sundsbø, 1998; Beyers et al., 2004; Tominaga et al., 2011a; Thiis and Ferreira, 2015; Zhou et al., 2016c). In comparison to wind-tunnel experiments and full-scale measurements, CFD can provide detailed information on the relevant flow variables in the whole computational domain, under well-controlled conditions and without similarity constraints (van Hooff and Blocken, 2010; Blocken, 2015; Tominaga, 2017). However, the physical processes of snow drifting are very complicated. Consequently, the accuracy and reliability of snow drifting simulations in CFD are of concern and special attention should be given to solution verification and validation studies. Detailed reviews were provided by Tominaga et al. (2011a) and Tominaga (2017) for CFD simulations of snow drifting from an engineering point of view. As the authors pointed out, most of the past research efforts concern application examples. A comprehensive sensitivity analysis for CFD simulations of snow drift is - to the best knowledge of the authors - still missing in the literature.

The Eulerian method is commonly adopted for simulation of snow drifting in engineering, for its low computational expense due to the addition of only one single set of equations. One additional term, the drift flux of snow, which represents the effect of gravitational sedimentation of snow in terms of the falling velocity w_f, is used in the governing equation for the snow phase. Tominaga et al. (2011) gave an overview of the numerical models used by previous researchers in the CFD simulation of snowdrift around buildings or structures. The governing equations for snow suspension are described as follows:

$$\frac{\partial \phi}{\partial t} + \frac{\partial \phi u_j}{\partial x_j} + \frac{\partial \phi w_f}{\partial x_3} = \frac{\partial}{\partial x_j} D_t \frac{\partial \phi}{\partial x_j} \tag{1}$$

$$D_t = \frac{\nu_t}{Sc_t} \tag{2}$$

where ϕ is the snow concentration; w_f is the falling velocity of snow; D_t is the turbulent diffusion coefficient; ν_t is the kinematic turbulent viscosity, and Sc_t is the turbulent Schmidt number.

The erosion or deposition of snow can be modeled by the calculation of the snow flux near the snow surface. The erosion-deposition model developed by Naaim et al. (1998) is most widely used (e.g. Beyers et al., 2004; Thiis et al., 2009; Zhou et al., 2016c):

$$q_{ero} = A_{ero}\left(u_*^2 - u_{*t}^2\right) \tag{3}$$

$$q_{dep} = \phi w_f \frac{u_{*t}^2 - u_*^2}{u_{*t}^2} \tag{4}$$

where A_{ero} is the erosion coefficient of snow reflecting the bonding strength of the snowpack; u_* is the friction velocity near the snow surface; u_{*t} is the threshold friction velocity of snow. A value of $A_{ero} = 7\times10^{-4}$ kg·m^4·s was given by Naaim et al. (1998) based on calibration using the field measurements of Takeuchi (1980).

From Eqs. (1)-(4), the key parameters that need to be specified in the numerical model for snow transport are the falling velocity of snow w_f, the turbulent Schmidt number Sc_t and the threshold friction velocity of snow u_{*t}. Table 1 presents a list of physical and computational parameters used by previous researchers which have yielded reasonable numerical results for their respective simulations. In the table, snow density ρ_s is used to calculate the variation of snow depth from the snow flux. CFD simulations of snow drifting are typically used for an application purpose with no systematic sensitivity study conducted. As recorded in Table 1, a wide range of values were used by previous researchers in their CFD simulations of snow drifting in the past: the falling velocity of snow w_f ranges from 0.20 m/s to 1.0 m/s, the threshold friction velocity of snow u_{*t} from 0.15 m/s to 0.36 m/s, and the snow density ρ_s from 50 kg/m^3 to 700 kg/m^3. A falling velocity of snow w_f of

0.50 m/s is the most commonly used value, while a turbulent Schmidt number of 1.0 was used in numerous snow drifting studies in CFD.

Table 2 reports values of the properties of snow and falling snow obtained from field measurements. Since the physical properties of snow are usually related to the particle diameter (d_p), the values of d_p are also listed in the table. The results from the field measurements for the physical properties of falling snow, as presented in Table 2, demonstrate that these parameters (falling velocity, threshold velocity, density, and particle diameter) can vary within a wide range. Although most values presented for CFD simulations in Table 1 are within the limits of the measurement results in Table 2, the differences between the values used by previous researchers remain obvious. The objective to obtain the best agreement between experimental and numerical results usually acts as the principle in determining the values of these parameters. It is widely recognized that the results of CFD simulations can be very sensitive to the wide range of computational parameters that are determined by the user prior to commencing a simulation(e.g. Franke et al., 2007; Tominaga et al., 2008; Ramponi and Blocken, 2012; Blocken, 2014; van Hooff et al., 2017). Although CFD predictions of snow drifting have been successfully used in several application cases, the impact of the physical and computational parameters on the results of snow-drifting simulations are not yet fully understood, and guidelines for CFD snow-drifting simulations are therefore required.

This paper presents a detailed analysis of the impact of several key physical and computational parameters on the results of CFD simulation of snow transport over flat, uniformly rough, open terrain, with emphasis on the fundamentals of snow transport prediction techniques. The simulations are validated by field measurement results by Pomeroy and Male (1992). The parameters include the grid resolution, the falling velocity of snow, the turbulent Schmidt number, the threshold friction velocity of snow and the turbulence model.

The numerical method used to predict snow transport over flat, uniformly rough, open terrain is presented in Section 2. In Section 3, the computational settings for the reference case are described. The verification and validation of the CFD simulation for the reference case are presented in Section 4. A systematic analysis of the impacts of several key physical and computational parameters is provided in Section 5. Finally, Sections 6 (discussion) and 7 (conclusions) conclude the paper.

2. Numerical method

2.1 Simulation scheme

The Eulerian-Eulerian approach is adopted in this study, i.e. both air and snow are treated as a continuum. The simulation scheme is illustrated in Fig. 1. In addition to the convection flux, the settling flux, diffusion flux and entrainment flux are also calculated (Fig. 1). The settling flux is defined by the additional term $\frac{\partial \phi w_f}{\partial x_3}$ in Eq. (1), which represents the effect of gravitational sedimentation of snow in terms of the falling velocity w_f as mentioned above. The diffusion flux is defined by the diffusion term $\frac{\partial}{\partial x_j} D_t \frac{\partial \phi}{\partial x_j}$ in Eq. (1), in which the diffusion coefficient D_t (Eq.(2)) needs to be specified. The entrainment flux, which represents the amount of snow that enters into the domain, is defined by the boundary condition of the snow surface (Eq. (8)).

Here, snow transport over flat, uniformly rough, open terrain is divided into two parts: snow saltation near the snow surface and snow suspension in the air. Creep is included in the simulation of snow saltation. This simulation method has been commonly used by previous researchers (e.g. Naaim et al., 1998; Sundsbø, 1998; Beyers et al., 2004). The boundary height between snow

saltation and snow suspension, namely the saltation height h_{sal}, is determined by Eq. (5), which was proposed by Pomeroy and Gray (1990) from a number of field measurements,

$$h_{sal} = 1.6\frac{u_*^2}{2g} \tag{5}$$

with g the gravitational constant.

2.2 Snow suspension

Eq. (1) is most frequently used in previous studies as the governing equation for the snow suspension and is also used in this study. Since steady simulations are conducted, the unsteady term ($\frac{\partial \phi}{\partial t}$) in Eq. (1) is omitted in this study and all values for concentrations, velocities, etc. are mean values in the remainder of this paper. Compared with the standard governing equation of mass transport, an additional term is used to consider the gravitational sedimentation of snow in terms of w_f.

2.3 Snow saltation

The governing equation of snow saltation is as follows:

$$\frac{\partial \phi u_j}{\partial x_j} = \frac{\partial}{\partial x_j} D_t \frac{\partial \phi}{\partial x_j} \tag{6}$$

The erosion flux per unit area from the snow surface to the flow domain is calculated by Eq. (3), in which the friction velocity is calculated from the following equation:

$$u_* = \sqrt{\tau_W / \rho_a} \tag{7}$$

with τ_w the shear stress near the snow surface and ρ_a the air density. Based on the CFD simulation results of air flow and the standard wall function (Launder and Spalding, 1974, Eqs. (20-22)), the wall shear stress τ_w can be obtained. In the simulation, the erosion flux is used as the surface boundary condition for the transport equation of snow, as shown in Eq. (8).

$$\frac{\nu_t}{Sc_t}\left(\frac{\partial \phi}{\partial z}\right)\Bigg|_{surface} = q_{ero} \tag{8}$$

Over flat, uniformly rough, open terrain, when snow transport becomes fully developed, the erosion and deposition of snow near the ground would also reach a state of equilibrium, and the snow concentration would remain almost unchanged downwind. Thus, Naaim et al. (1998) used the following relation to modify the friction velocity near the snow surface, which was referred to as the assumption of Kind (1975): the shear stress at steady state of snow transport must remain at the threshold value in order to maintain a "mobile" bed.

$$u_{*,r} = u_* + \left(u_{*_t} - u_*\right)\left(\frac{\phi}{\phi_{\max}}\right)^2 \tag{9}$$

with $u_{*,r}$ the real friction velocity that is used in the simulation of snow transport and $\phi_{\max}$ the maximum snow concentration in the saltation layer.

The maximum snow concentration in the saltation layer can be estimated through the semi-empirical relationships proposed by Pomeroy and Gray (1990):

$$Q_{sal} = \frac{0.68\rho_a u_{*t}}{g u_*}\left(u_*^2 - u_{*t}^2\right) \tag{10}$$

with Q_{sal} the snow transport rate in the equilibrium state of snow transport. The saltation velocity (u_{sal}) is determined by the following equation (Pomeroy and Gray, 1990):

$$u_{sal} = 2.8u_{*t} \tag{11}$$

From the relationship $Q_{sal} = \phi_{sal} h_{sal} u_{sal}$, the maximum snow concentration in the saltation layer can be estimated as:

$$\phi_{\max} = \phi_{sal} = \frac{Q_{sal}}{h_{sal} u_{sal}} = \frac{\rho_a}{3.29u_*}\left(1 - \frac{u_{*t}^2}{u_*^2}\right) \tag{12}$$

where the saltation height is given by Eq. (5). Eq. (12) was also used by Naaim et al. (1998) to calculate the maximum snow concentration in CFD simulations of snow transport.

3. Computational settings and parameters: reference case

3.1 Computational domain and grid

The simulation of snow transport is performed in 2D and at full scale. A comparison between 2D simulation and 3D simulation results is made to ensure that a 2D simulation is sufficient for the sensitivity analysis (Section 4.1.2). The dimension of the computational domain in this study is 3 km (L) x 10 m (H), as illustrated in Fig. 2a (figure not to scale). During snow transport, the snow concentration of suspension above 1 m from the snow surface is already very small. Therefore, the height of the computational domain is set to 10 m. A length of 3000 m for the computational domain is sufficient for fully-developed snow transport over flat, uniformly rough, open terrain.

A structured grid with a high spatial resolution near the ground is created. For the reference case, the horizontal and vertical stretching ratios are 1.10 and 1.05, respectively. The vertical minimum grid size near the ground is 0.008 m and the horizontal minimum grid size is 0.30 m. The total grid consists of 211,000 cells. The computational settings for the reference case are summarized in Table 3.

3.2 Boundary conditions

A logarithmic vertical mean wind speed profile is imposed at the inlet:

$$U(z) = \frac{u_{\mathrm{ABL}}^*}{\kappa}\ln\left(\frac{z}{z_0}\right) \tag{13}$$

with u^*_{ABL} the atmospheric boundary layer (ABL) friction velocity, κ the von Karman constant (0.42) and z the vertical height above the ground (snow surface). A constant profile of turbulent kinetic energy (Richards and Hoxey, 1993) is used (Eq. (14)), whereas turbulence dissipation rate ε is calculated by Eq. (15), with C_μ an empirical constant equal to 0.09.

$$k(z) = \frac{u^{*2}_{ABL}}{\sqrt{C_\mu}} \tag{14}$$

$$\varepsilon(z) = \frac{u^{*3}_{ABL}}{\kappa z} \tag{15}$$

The aerodynamic roughness length of the surface during snow transport is calculated with the empirical equation from the field measurement by Pomeroy and Gray (1990):

$$z_0 = 0.1203\frac{u_*^2}{2g} \tag{16}$$

The specific dissipation rate ω for the k-ω model, which is used in the sensitivity analysis of the turbulence model in Section 5.5, is calculated using Eq. (17):

$$\omega(z) = \frac{\varepsilon(z)}{C_\mu k(z)} \tag{17}$$

In the simulation using the RSM turbulence model, the Reynolds-stress components are approximately determined from the specified values of k. The turbulence is assumed to be isotropic such that(ANSYS Inc, 2016)

$$\overline{u_i' u_j'} = 0 \tag{18}$$

and

$$\overline{u_\alpha' u_\alpha'} = \frac{2}{3}k \tag{19}$$

(no summation over the index α).

The ground surface, namely the surface of snowpack, is set as no-slip wall, and standard wall functions (Launder and Spalding, 1974) with sand-grain based roughness modification (Cebeci and Bradshaw, 1977) are used. The specific expression for the standard wall function is (ANSYS Inc, 2016):

$$U^+ = \frac{1}{\kappa}\ln\left(Ey^+\right) \tag{20}$$

where

$$U^+ = \frac{U_P C_\mu^{1/4} k_P^{1/2}}{\tau_w / \rho_a} \tag{21}$$

is the dimensionless velocity.

$$y^+ = \frac{\rho_a C_\mu^{1/4} k_P^{1/2} y_P}{\mu} \tag{22}$$

is the dimensionless distance from the wall. In Eqs. (20-22), E is an empirical constant (= 9.793); U_p is the mean velocity of the fluid at the near-wall node P; k_P is the turbulence kinetic energy at the near-wall node P; y_P is the distance from point P to the wall, and μ is the dynamic viscosity of the air flow.

As mentioned above, the aerodynamic roughness length of the surface z_0 (= 5.90×10^{-4} m) can be calculated from Eq. (16). Using their consistency relationship with z_0 as derived by Blocken et al. (2007), the sand-grain roughness height can be calculated as: $k_S = 9.793 z_0 / C_S$, with a selected value of the roughness constant C_S = 2.0. The values of the sand-grain roughness height k_S (m) and the roughness constant C_S are also summarized in Table 3.

Zero static gauge pressure is imposed at the outlet. The upper boundary of the domain is set as symmetry, i.e. zero normal velocity and zero normal gradients of all variables.

3.3 Solver settings and computational parameters

The commercial CFD software ANSYS Fluent 17.2 is employed in this study with additional user-defined functions to simulate the transport of snow particles. The steady Reynolds-averaged Navier-Stokes (RANS) equations are solved with the realizable k-ε turbulence model by Shih et al. (1995). The SIMPLE algorithm is used for pressure-velocity coupling, pressure interpolation is standard and second-order discretization schemes are used for both the convection terms and the viscous terms of the governing equations. Convergence is assumed to be obtained when all the scaled residuals level off and reach a minimum of 10^{-11} for continuity, 10^{-14} for x velocity, y velocity, k and ε, and 10^{-15} for snow with the use of a double precision solver.

The parameters relating to the properties of snow and falling snow for the reference case are given in Table 4. Values of the threshold friction velocity u_{*t} and friction velocity u_* are adopted from the field measurements by Pomeroy and Male (1992). As in most previous studies, the turbulent Schmidt number Sc_t is set as 1.0 (see Table 1). During snow transport, in the higher part above the snow surface, snow particles tend to have a small diameter and a small falling velocity. Moreover, from the observation of the measurement results of snow transport over flat, uniformly rough, open terrain, snow concentration rapidly decreases in the vertical direction when the height above the snow surface is lower than around 0.1 m. On the other hand, if the height is larger than 0.1 m, the amplitude of variation for snow concentration is not that large in the lower part ($z \leq$ 0.1 m). Based on this judgement, a switching height of 0.1 m in the suspension layer is used. Hence, in the higher part ($z >$ 0.1 m) a relatively low falling velocity (w_f = 0.24 m/s) is applied, while in the lower part ($z \leq$ 0.1 m) a high falling velocity (w_f = 0.48 m/s) is used. The switching height and the falling velocities are constant along the horizontal direction. From the validation results in Section 4.2, the values of switching height and falling velocity seem appropriate for the reference case.

4. Verification and validation

Before validation and sensitivity analysis, the verification of the horizontally homogeneous atmospheric boundary layer (ABL) and an analysis of the impact of the dimensions of the computational domain are conducted. The field measurement data from Pomeroy and Male (1992) are used to validate the CFD simulation results for the reference case.

4.1 Verification

4.1.1 Check of horizontal homogeneity

Accurate simulation of ABL flow in the computational domain is imperative to obtain accurate and reliable predictions of the related atmospheric processes (Richards and Hoxey, 1993; Blocken et al., 2007), among which snow transport. To obtain a horizontally homogeneous ABL, two measures are used in all simulations: (1) along the length of the top boundary, the values from the inlet profiles of U, k and ε are fixed as constant in the top layer of cells in the domain; (2) wall shear stress is specified at the bottom boundary in the domain, which is calculated from the equation $\tau_w = \rho_a {u^*}_{ABL}^2$ (Blocken et al., 2007).

Fig. 3 depicts the horizontal homogeneity check for the wind profiles at three separate locations, namely at the inlet (x = 0 m), at x = 1000 m and at x = 2000 m. The dimensionless mean wind speed (U/U_H), dimensionless turbulent kinetic energy (k/k_H) and dimensionless turbulent dissipation rate ($\varepsilon/\varepsilon_{max,inlet}$) are compared. The wind profiles are almost identical at these three locations (the discrepancies within 1.5%). Note that the wind profiles are only compared for the reference case in Fig. 3, in which the realizable k-ε model is applied. More information on the horizontal homogeneity for other turbulence models is provided in Section 5.5.

4.1.2 Comparison between 2D and 3D

Fig. 4 compares the predicted snow concentrations along the height obtained from 2D and 3D simulations. For the 3D simulation, the width of the domain is 1 m, and ten cells are used in the third direction. All the settings of the 3D simulation are identical to those of 2D simulations. Fig. 4 demonstrates that the 2D and 3D CFD simulation results are nearly identical. There is only a negligible difference (the percentage difference for the largest snow concentration is 0.02%) recorded between the result from the 2D simulation and 3D simulation. Therefore, only 2D simulations are performed in this study for the following analysis.

4.2 Validation

4.2.1 Snow concentration near the ground

A minimum fetch distance is required for snow transport to become fully developed. Tabler (2003) gave a reduction factor to take into account the limited fetch distance for snow transport rate based on field measurements. Here, this empirical relationship is used to analyze the numerical results. According to the reduction relation proposed by Tabler (2003), the snow concentration near the ground could be determined from:

$$\phi(x) = \phi_{max}\left(1 - 0.14^{x/F}\right) \tag{23}$$

where x is the fetch distance from the starting point; F is the minimum fetch distance for fully-developed snow transport. In the field measurements (Pomeroy and Male, 1992), the value of F was not measured. Therefore, the value of F needs to be determined from the CFD simulation results. From Eq. (23), it is evident that when the fetch distance x is equal to the minimum fetch distance for the fully-developed snow transport F, the reduction factor for the maximum snow concentration is 0.86. Hence, the value of F can be calculated as 417 m (distance to reach 86% of the maximum snow concentration) from the CFD simulation results, which could be determined in Fig. 5. In Fig. 5, the snow concentration at the first cell adjacent to the snow surface (z = 0.004 m) is used as the snow concentration near the snow surface in the CFD simulation. Fig. 5 demonstrates that the variation of snow concentration along a horizontal line near the snow surface from the CFD simulation is very close to that of the empirical relation obtained from field measurements. It can

be concluded that in this particular case the modification method for friction velocity as presented in Eq. (9) results in a prediction of snow concentration over flat, uniformly rough, open terrain by CFD that is similar to the results from the empirical relation established by Tabler (2003).

4.2.2 Vertical distribution of snow concentration

Pomeroy and Male (1992) presented measurement results of snow transport over flat, uniformly rough, open terrain. The site was located 4 km west of Saskatoon, Canada. Field measurements were conducted in January 1987, where vertical profiles of the flux of suspended snow particles, mean wind speed, air temperature and humidity were determined from 7.5 minute averaged measurements over a plain uniform surface of summer fallow (soil cultivated so that all vegetation is removed) overlain by complete snow cover (Pomeroy and Male, 1992). The level heights for the measurement of snow concentration were logarithmically spaced from 0.01 m to 2 m. The threshold friction velocity and friction velocity derived from the on-site measurements that are used for the simulation of the reference case are shown in Table 4.

Fig. 6 illustrates the spatial distribution of snow concentration from the CFD simulation. As in the field measurement, only the results below 1 m are demonstrated, since the snow concentrations at higher positions are very small. Snow transport reaches equilibrium ahead of 1000 m downwind of the starting point, since the near-wall snow concentration reaches 99.9% of the highest downwind snow concentration based on the simulation results shown in Fig. 5. Depending on the snow conditions and location, it is possible for the minimum fetch distance for fully developed snow transport to vary over a wide range. Tabler (2003) reported a distance of 3 km in Wyoming for the minimum fetch distance, which is considerably different from the 210 m measured by Takeuchi (1980). A development length of 1 km seems reasonable in this case. Along the vertical coordinate direction, snow concentration drops rapidly in orders of magnitude.

An analysis of the snow concentration is conducted for the equilibrium state of snow transport. As shown in Fig. 6, at x = 2000 m snow transport has reached its equilibrium. Therefore, this location (x = 2000 m) is chosen to compare the vertical distribution of snow concentration during snow transport between CFD simulation and field measurement in Fig. 7. Since snow concentration rapidly decreases in vertical direction, a logarithmic scale is adopted for the horizontal axis depicting the snow concentration. The grid-convergence index (GCI) as proposed by Roache (1994, 1997) is also shown in Fig. 7. The specific calculation procedure of GCI can be seen in Section 5.1.

Measurements of snow concentration profiles are characterized by an exponential decrease in mass concentration with height resulting in values at 1 m height which are three to four orders of magnitude smaller than those near the surface (Pomeroy and Male, 1992). Generally, the CFD results agree well with the measured data for the snow concentration in the air. The deviations between CFD simulation and field measurement results are within 0.1 g/m^3 at higher locations ($z >$ 0.1 m), and the average percentage difference is 9.4%. At lower locations ($z \leq 0.1$ m), the snow concentration drops rapidly with about three orders of magnitude with increasing height compared to the value at the first cell adjacent to the snow surface. In the higher part of the flow domain, due to a very low snow concentration in the air, the decrease becomes smaller with only about one order of magnitude decrease from 0.1 m to 1 m.

The snow concentration predicted by CFD is lower than the measured value in the lower part ($z \leq 0.1$ m). This underestimated snow concentration might be caused by the underestimation of the diffusion of snow in this zone, i.e. a relatively large value of turbulent Schmidt number ($Sc_t = 1.0$) is applied for the lower part. Given the high snow concentration gradient near the surface, the diffusion of snow should be pronounced. However, due to a lack of measurement data to aid in defining the turbulent Schmidt numbers for snow transport, the most commonly used value of $Sc_t = 1.0$ is applied in the reference case. In Section 5.3, the impact of turbulent Schmidt number on the CFD simulation results will be discussed. Another reason might be the overestimation of the

falling velocity of snow w_f, i.e. the overestimation of settling flux of snow in the lower part. The impact of falling velocity of snow on the CFD simulation results will be discussed in Section 5.2.

5. Sensitivity analysis

Sensitivity analyses are performed to analyze the impact of the grid resolution, the falling velocity of snow (w_f), the turbulent Schmidt number (Sc_t), the threshold friction velocity of snow (u_{*t}) and the turbulence model, starting from the reference case. To study the impact of one physical or computational parameter, all the other physical and computational parameters and solver settings are kept identical to the reference case.

5.1 Impact of grid resolution

A grid-sensitivity analysis is performed with the realizable k-ε model (Shih et al., 1995). The simulations should show no or negligible differences in the results when refining the grid size starting from the reference case (= 105 cells along the height). The minimum horizontal grid size is 0.30 m for all grids assessed in this study, however, the number of grid cells is varied in the vertical height (10 m) of the flow domain, ranging from 30 to 120 with an identical minimum grid size in vertical direction (= 0.008 m) for the wall-adjacent cell. Fig. 8 shows the profiles of snow concentration over height, indicating that the impact of vertical grid size on the simulation results can be pronounced. When the number of grid cells in the vertical direction is equal or larger than 90, the simulation results are nearly grid-converged. Therefore, all the simulations are conducted with 105 cells in the vertical direction.

To quantify the uncertainty from grid resolution, the grid-convergence index (GCI) as proposed by Roache (1994, 1997) is used:

$$\mathrm{GCI} = F_s \left| \frac{r^p \left(f_2 - f_1 \right)}{1 - r^p} \right| \tag{24}$$

with F_s the safety factor, taken to be 1.25, r the grid refinement factor, p the formal order of accuracy which is assigned as 2 for the second-order upwind discretization scheme, f_1 the CFD simulation results from the coarse grid and f_2 the CFD simulation results from the fine grid. Here the grids with 60, 90 and 120 cells along the vertical direction are used to calculate the GCI for the reference grid. Fig. 9 illustrates the calculated results of the largest GCI for the snow concentration, which is in relation to the grid of 60 cells. Compared with the relatively low values of the GCI in the lower part ($z \leq 0.1$ m), the GCI in the higher part is pronounced ($z > 0.1$ m). With the increase of height, the GCI also increases. The largest GCI is 0.12 g/m^3 in the higher part ($z > 0.1$ m).

5.2 Impact of falling velocity of snow

To investigate the impact of the falling velocity of snow (w_f), the constant values that were used in previous studies (Table 1) are tested in the sensitivity analysis. The CFD simulation results are shown in Fig. 10. The falling velocity of snow has a very large influence on the vertical distribution of snow concentration during snow transport. There is an equilibrium balance in the suspension layer between upward transport by turbulent diffusion and downward settling of particles due to gravity (Naaim-Bouvet et al., 2013), as illustrated in Fig. 1. As the falling velocity increases, the settling flux would restrain the diffusion of snow. Therefore, the snow concentration by the CFD simulation decreases significantly with the increase in the falling velocity of snow w_f.

In this case (Sc_t = 1.0), a falling velocity between 0.30 m/s and 0.45 m/s provides the best agreement between numerical results and results from the field measurement. A settling velocity of 0.50 m/s is the most common value selected by other researchers (e.g. Uematsu et al., 1991;

Tominaga and Mochida, 1999; Beyers et al., 2004; Thiis et al., 2009; Potac and Thiis, 2011; Tominaga et al., 2011b), which presents close results to those of field measurements in the lower part ($z \leq 0.15$ m).

The snow concentration in the lower part is believed to be important for the prediction of snow drifting around or on buildings. Fig. 11 presents the impact of the falling velocity w_f on the vertical distribution of drifting snow in the lower part of the domain ($z \leq 0.15$ m). At 0.12 m, the snow concentration predicted by w_f = 0.50 m/s is within the error of 0.1 g/m^3 compared to the measurement results. Cases with w_f = 0.30 m/s, 0.20 m/s and 1.00 m/s present deviations of about one to two orders of magnitude. From the measurement results of physical properties of snow particles from literature (Table 2), the value of w_f = 0.50 m/s might correspond to snow particle diameters larger than 1 mm. However, it should be pointed out that the falling velocity of snow particles is not only dependent on the particle diameter; other environment parameters such as temperature or humidity can also have a large impact on this value.

5.3 Impact of turbulent Schmidt number

The turbulent Schmidt number Sc_t is a very important parameter in the prediction of mass transfer if the Eulerian approach is adopted (e.g. Tominaga and Stathopoulos, 2007). Values of Sc_t = 0.5, 0.7, 1.0, 1.3 and 1.5 are tested in this study. The measurement data from Naaim-Bouvet et al. (2013) indicated that the turbulent Schmidt number of snow ranges from 0.5 to 1.3. A turbulent Schmidt number Sc_t of 1.0 is by far the most commonly used value in previous CFD simulations of snow drifting (Table 1).

Fig. 12 presents the impact of Sc_t on the vertical distribution of drifting snow. An increase of Sc_t would decrease the turbulent diffusion coefficient D_t ($D_t = \nu_t/Sc_t$), thus resulting in a decrease of snow concentration in the flow domain. The predicted snow concentrations are all smaller than the measured values when Sc_t is larger than 1.0. Sc_t = 1.5 results in an underprediction of snow concentration by CFD with approximately one to two orders of magnitude in the higher part ($z \geq$ 0.1 m). On the other hand, $Sc_t < 1.0$ would lead to the overprediction of snow concentration in general, and in the higher part ($z \geq 0.1$ m) in particular. Sc_t = 0.5 results in an overprediction of the snow concentration by CFD with approximately one to two orders of magnitude in the higher part ($z \geq 0.1$ m).

At z = 0.12 m, the snow concentration predicted by CFD is one order of magnitude larger than the measured values for Sc_t = 0.5 and about one order of magnitude smaller than the measurement results for Sc_t = 1.5. The deviations between CFD simulation and field measurement results would increase with increasing height. The sensitivity analysis in this section indicates that 1.0 could be a reasonable value for Sc_t in this case.

5.4 Impact of threshold friction velocity

For the reference case, the measured value of threshold friction velocity (u_{*t}) of 0.27 m/s is used, as stated in Section 3.3. However, the threshold condition of snow can vary within a wide range under different environmental conditions. Fig. 13 and 14 show the impact of the value of u_{*t} on the vertical distribution of snow concentration in the air. According to Eq. (12), when u_{*t} decreases, the amount of snow that is entrained into the flow domain increases. Therefore, the snow concentration is larger in the air for lower u_{*t}. At z = 0.12 m, the snow concentrations predicted by u_{*t} = 0.05 m/s is three times than that from u_{*t} = 0.25 m/s. The impact of u_{*t} is smaller than the impact of w_f and Sc_t, for the ranges indicated (5.2 and 5.3).

Fig. 15 shows the large impact of u_{*t} on the horizontal distribution of snow concentration at the first cell adjacent to the snow surface. A decrease of u_{*t} from 0.25 m/s to 0.05 m/s results in an increase of the saturated snow concentration at the first cell adjacent to the snow surface from 420 g/m^3 to 1168 g/m^3. Meanwhile, the fetch distance also slightly becomes larger with the increase

of near-ground snow concentration. An analysis of snow saltation (Pomeroy and Gray, 1990) suggests that mean mass concentrations in the saltation layer tend to fall between 400 and 900 g/m^3. Note that a value of u_{*t} = 0.05 m/s is considered to be very small. Even for dry and fresh snow, the value of u_{*t} is usually larger than 0.10 m/s (Table 1). Thus, in the simulations the maximum snow concentration near the snow surface is usually lower than 1000 g/m^3 and larger than 400 g/m^3, which corresponds to the measurement results of Pomeroy and Gray (1990).

As it is discussed in Section 1, the threshold friction velocity of snow can be influenced by many environmental factors, which can vary in a wide range, as shown in Table 2 in the paper. Kind (1990) pointed out that the threshold friction velocity for loose fresh dry snow at less than -2.5 °C can be lower than 0.15 m/s. The value 0.05 m/s is indeed very low for real snow, and chances are low that it would occur in reality. However, we obtained this value in an experiment in a climatic wind tunnel for dry tiny snow particles (d_p = 0.1 mm) during snowfall at -10 °C. Since this study focus on the sensitivity analysis, the results of 0.05 m/s have been retained in the paper.

5.5 Impact of turbulence model

Five steady RANS turbulence models are tested in this study: the realizable k-ε model (Shih et al., 1995), the renormalization group (RNG) k-ε model (Yakhot et al., 1992), the standard k-ε model (Jones and Launder, 1972), the Reynolds stress model (RSM, Launder et al., 1975) and the standard k-ω model (Wilcox, 1998). The impact of the turbulence model on the snow concentration at x = 2000 m is depicted in Fig. 16. The realizable k-ε, RNG k-ε and standard k-ω turbulence models provide very similar snow concentrations. Simulation results of the standard k-ε model display some deviations from the measurement results, while the RSM model exhibits the worst agreement.

The physical and computational parameters in the sensitivity analysis of turbulence models are identical to the reference case. Therefore, the deviations from different turbulence models probably originate from the differences in the prediction of turbulent diffusion of snow. As stated earlier, the turbulent diffusion coefficient of snow D_t is proportional to the turbulent viscosity ν_t because Sc_t is held constant. The Boussinesq hypothesis is used by the k-ε models and the k-ω models (ANSYS Inc, 2016). The turbulent viscosity ν_t in the k-ε models is computed by combining k and ε as displayed in Eq. (25), while ν_t in the k-ω models is computed as a function k and ω as displayed in Eq. (26). For the Reynolds stress models based on the ε-equation, the turbulent viscosity, ν_t, is computed similarly to the k-ε models, namely using Eq. (25).

$$k-\varepsilon \text{ models}: \ \nu_t = \rho_a C_\mu \frac{k^2}{\varepsilon} \tag{25}$$

$$k-\omega \text{ models}: \ \nu_t = \alpha^* \frac{\rho_a k}{\omega} \tag{26}$$

with α^* a coefficient that damps the turbulent viscosity in the k-ω model.

Analysis of the ABL profiles at different locations demonstrates that the mean velocity profile and turbulence dissipation rate profile remain almost unchanged along the streamwise direction. The results for the profiles of U and ε are similar to Fig. 3a,c as shown in Fig. 17a-e. No streamwise gradients are present except for the profiles obtained with the RSM turbulence model. In addition, the profiles of turbulent kinetic energy do show some deviations between the turbulence models tested at the downwind locations, as shown in Fig. 17. The standard k-ε turbulence model slightly overestimates the turbulent kinetic energy at the two downstream locations compared to k at the inlet, while the standard k-ω model slightly underestimates the turbulent kinetic energy. The input of k and ε profile at the inlet and the use of standard wall functions cannot guarantee a horizontally

homogeneous profile of turbulent kinetic energy for the RSM turbulence model used in the study. Near the ground, RSM predicts much larger turbulent kinetic energy values (20% increase compared to inlet value) (Fig. 17d), which leads to high snow concentrations (Fig. 16) in the CFD simulation due to a higher estimation of turbulent viscosity ν_t (Eqs. (25-26)), and thus also a higher turbulent diffusion of snow (given the same Sc_t), as shown in Fig. 16. As a result, the change in turbulent kinetic energy profile by the RSM model does not allow a proper prediction of snow transport.

6. Discussion

This paper presented CFD simulations of snow transport over flat, uniformly rough, open terrain with an Eulerian method that is commonly used for snow drifting around buildings or on building roofs. A sensitivity analysis of several key physical and computational parameters was conducted. While the study gives insights for future CFD simulations of snow transport, it is also important to mention the limitations of this study.

1) Since the numerical model was proposed and applied for engineering purposes, some physical processes are simplified or ignored within the numerical model. The physical properties of snow for the simulation are assumed to be constant, which is not always the case in reality. In addition, thermodynamic effects, such as sublimation of snow during snow transport, have not been taken into account, although these are often considered in the meteorological field. The effects of snow transport on the wind flow were also not considered within the methodology used in this study.
2) Although the numerical model used in this study has shown accurate and reliable in reproducing snow transport over flat, uniformly rough, open terrain, the applicability of the numerical model should be extensively validated and the sensitivity analysis should be extended for complex configurations and for building roofs.
3) In this study, a switching height of 0.1 m in the suspension layer is used in the CFD simulation for the reference case. The validation study in Section 4.2.2 demonstrates that reasonable results can be obtained using this switching height. However, it should be pointed out that the value of switching height can be influenced by certain environmental factors, such as wind velocity. For example, under stronger wind, the switching height could be larger than 0.1 m. The numerical model used for the reference case in this study is a simplified model. This study does not investigate the influence of switching height on the simulation results. For future study, when using this numerical model, the switching height should be determined based on the actual situation and an extra validation study.

It is recommended that detailed information will be recorded during future on-site measurement campaigns of snow drifting or snow transport, such as snow concentration or snow flux in the concerning region, falling velocity of snow and threshold friction velocity of snow. Since detailed information can be obtained from CFD simulations, then the snowdrift predictions can be validated by these on-site full-scale measurements of snow concentration or snow flux in addition to snowdrift patterns for future research. This would provide more insights regarding the model development.

7. Summary and conclusions

Accurate and reliable CFD simulations of snow concentrations in snow transport are essential for many practical applications such as visibility prediction during snow transport and snowdrift evaluation around buildings or on building roofs in engineering applications. A review of the literature indicates the adoption of a wide range of key physical and computational parameters. This paper presents an analysis of the impact of several of those parameters on the CFD simulation

of snow transport over flat, uniformly rough, open terrain, and is intended to guide future simulation efforts. The following conclusions have been obtained:

1) A correct specification of ABL inlet profiles and the avoidance of unintended streamwise gradients (horizontal inhomogeneity) is very important. It is found that a change in vertical turbulent kinetic energy profile can have a large effect on the predicted snow concentrations, leading to large deviations with experimental values.
2) By means of a sensitivity analysis for the grid resolution, it is found that a minimum vertical grid size of 0.008 m with a stretching ratio 1.05 is sufficiently fine for the grid in the vertical direction. These settings are found to provide reasonable results in the simulation of snow transport over flat, uniformly rough open terrain.
3) In engineering applications, usually only one set of constant physical and computational parameters is used for CFD simulations of snow transport. The sensitivity analysis of falling velocity of snow demonstrates that the application of one such set can reproduce snow transport accurately, but only if proper values are used.
4) If the Eulerian method is used to predict snow transport in air, special care should be taken to choose appropriate values for the falling velocity of snow. From the sensitivity analysis conducted in this study, w_f = 0.2-0.5 m/s is found to be accurate if a turbulent Schmidt number of 1.0 is used. A value of 1.0 m/s for w_f might be too large for the suspending snow in air.
5) Detailed experimental data for turbulent mass diffusivities or the related turbulent Schmidt numbers is currently not available in the literature. However, based on the sensitivity analysis of Sc_t, the assumption of Sc_t = 1.0 seems to be appropriate for the CFD simulation of snow transport over flat, uniformly rough, open terrain. A higher or lower value of the turbulent Schmidt number can have a significant influence on the simulation results.
6) The threshold friction velocity is one of the most important parameters in the CFD simulation of snow transport. The value of u_{*t} significantly affects snow concentration in the saltation layer. u_{*t} should be determined from field measurements. If field measurement data are not available and cannot be acquired, this value should be determined based on information on the situation that is to be numerically addressed. For example, ground snow after snowfall concurrent with rain, typically corresponds to a higher threshold friction velocity (higher than 0.25 m/s). On the other hand, for fresh dry snow in a cold environment, the threshold friction velocity could be lower than 0.15 m/s.
7) It has been shown that the choice of turbulence model and the grid resolution can affect the vertical profiles of turbulent kinetic energy, which is a key factor influencing snow transport. Apart from the RSM turbulence model, a relatively horizontally homogeneous ABL could be obtained with the k-ε models and standard k-ω model. However, due to the pronounced overestimation of turbulent kinetic energy near the ground, the RSM significantly overestimates the snow concentration in the lower part of the domain. In future research and applications on snow transport, special care should be paid to choosing a proper turbulence model to obtain the best prediction of turbulent kinetic energy.

Acknowledgements

The research is supported by the National Natural Science Foundation of China (51778492, 51478359). The first author's work was also supported by the Chinese Scholarship Council (CSC) during his visit to the Department of the Built Environment of Eindhoven University of Technology. Twan van Hooff is a postdoctoral fellow of the Research Foundation—Flanders (FWO) at KU Leuven, in Flanders, Belgium (project FWO 1.2.R97.18N), its financial support is gratefully acknowledged. The authors also gratefully acknowledge the partnership with ANSYS CFD.

References

Alhajraf, S., 2004. Computational fluid dynamic modeling of drifting particles at porous fences. Environ. Model. Softw. 19, 163–170.

ANSYS Inc, 2016. ANSYS Fluent 17.0 Theory Guide, Ansys Inc.

Beyers, M., Harms, T.M., 2003. Outdoors modelling of snowdrift at SANAE IV Research Station, Antarctica. J. Wind Eng. Ind. Aerodyn. 91, 551–569.

Beyers, M., Sundsbø, P.A., Harms, T.M., 2004. Numerical simulation of three-dimensional, transient snow drifting around a cube. J. Wind Eng. Ind. Aerodyn. 92, 725–747.

Beyers, M., Waechter, B., 2008. Modeling transient snowdrift development around complex three-dimensional structures. J. Wind Eng. Ind. Aerodyn. 96, 1603–1615.

Blocken, B., Stathopoulos, T., Carmeliet, J., 2007. CFD simulation of the atmospheric boundary layer: wall function problems. Atmos. Environ. 41, 238–252.

Blocken, B., 2014. 50 years of Computational Wind Engineering: Past, present and future. J. Wind Eng. Ind. Aerodyn. 129, 69–102.

Blocken, B., 2015. Computational Fluid Dynamics for urban physics: Importance, scales, possibilities, limitations and ten tips and tricks towards accurate and reliable simulations. Build. Environ. 91, 219–245.

Cebeci, T., Bradshaw, P., 1977. Momentum transfer in boundary layers, McGraw-Hill Book Co.

Cierco, F.-X., Naaim-Bouvet, F., Bellot, H., 2007. Acoustic sensors for snowdrift measurements: How should they be used for research purposes? Cold Reg. Sci. Technol. 49, 74–87.

Doorschot, J.J.J., Lehning, M., Vrouwe, A., 2004. Field measurements of snow-drift threshold and mass fluxes, and related model simulations. Boundary-Layer Meteorol. 113, 347–368.

Franke, J., Hellsten, A., Schlünzen, H., Carissimo, B., 2007. Best practice guideline for the CFD simulation of flows in the urban environment, COST action.

Gray, D.M., Male, D.H., 1981. Handbook of snow: principles, processes, management & use. Pergamon Press.

Huang, Q., Hanesiak, J., Savelyev, S., Papakyriakou, T., Taylor, P.A., 2008. Visibility during Blowing Snow Events over Arctic Sea Ice. Weather Forecast. 23, 741–751.

Irwin, P.A., Gamble, S.L., Taylor, D.A., 1995. Effects of roof size, heat transfer, and climate on snow loads: studies for the 1995 NBC. Can. J. Civ. Eng. 22, 770–784.

Isyumov, N., Mikitiuk, M., 1990. Wind tunnel model tests of snow drifting on a two-level flat roof. J. Wind Eng. Ind. Aerodyn. 36, 893–904.

Jones, W.P., Launder, B.E., 1972. The Prediction of Laminarization with a Two-Equation Model of Turbulence. Intl. J. Heat Mass Tans. 15, 301–314.

Kajikawa, M., 1975. Experimental formula of falling velocity of snow crystals. J. Meteorol. Soc. Japan 53, 267–275.

Kind, R.J., 1975. A critical examination of the requirements for model simulation of wind-induced erosion/deposition phenomena such as snow drifting. Atmos. Environ. 10, 219–227.

Kind, R.J., 1986. Snowdrifting: A review of modelling methods. Cold Reg. Sci. Technol. 12, 217–228.

Kind, R.J., 1990. Mechanics of aeolian transport of snow and sand. J. Wind Eng. Ind. Aerodyn. 36, 855–866.

Launder, B.E., Spalding, D.B., 1974. The numerical computation of turbulent flows. Comput. Methods Appl. Mech. Eng. 3, 269–289.

Launder, B.E., Reece, G.J., Rodi, W., 1975. Progress in the development of a Reynolds-stress turbulence closure. J. Fluid Mech. 68, 537.

Liu, D., Yongle Li, B., Bin Wang, B., Peng Hu, B., Jingyu Zhang, B., 2016. Mechanism and effects of snow accumulations and controls by lightweight snow fences. J. Mod. Transp.

Matsuzawa, M., Kajiya, Y., Takeuchi, M., 2005. The development and validation of a method to estimate visibility during snowfall and blowing snow. Cold Reg. Sci. Technol. 41, 91–109.

Naaim-Bouvet, F., Naaim, M., Michaux, J.-L., 2002. Snow fences on slopes at high wind speed: physical modelling in the CSTB cold wind tunnel. Nat. Hazards Earth Syst. Sci. 2, 137–145.
Naaim-Bouvet, F., Bellot, H., Naaim, M., Nishimura, K., 2013. Size distribution, Schmidt number and terminal velocity of blowing snow particles in the French Alps : comparison with previous studies, in: International Snow Science Workshop (ISSW). pp. 140–146.
Naaim, M., Naaim-bouvet, F., Martinez, H., 1998. Numerical simulation of drifting snow: erosion and deposition models. Ann. Glaciol. 26, 191–196.
Nakaya, U., Terada, T.J., 1935. Simultaneous observations of the mass, falling velocity and form of individual snow crystals. J. Fac. Sci. Hokkaido Imp. Univ. 1, 191–200.
O'Rourke, M., Auren, M., 1997. Snow loads on gable roofs. J. Struct. Eng. 123, 1645–1651.
O'Rourke, M., DeGaetano, A., Tokarczyk, J.D., 2004. Snow drifting transport rates from water flume simulation. J. Wind Eng. Ind. Aerodyn. 92, 1245–1264.
O'Rourke, M., DeGaetano, A., Tokarczyk, J.D., 2005. Analytical simulation of snow drift loading. J. Struct. Eng. 131, 660–667.
Pomeroy, J.W., Gray, D.M., 1990. Saltation of Snow. Water Resour. Res. 26, 1583–1594.
Pomeroy, J.W., Male, D.H., 1992. Steady-state suspension of snow. J. Hydrol. 136, 275–301.
Potac, J., Thiis, T.K., 2011. Numerical simulation of snow drift development on a gabled roof, in: The 13th International Conference on Wind Engineering. Amsterdam, the Netherlands.
Ramponi, R., Blocken, B., 2012. CFD simulation of cross-ventilation for a generic isolated building: Impact of computational parameters. Build. Environ. 53, 34–48.
Richards, P.J., Hoxey, R.P., 1993. Appropriate boundary conditions for computational wind engineering models using the k-ϵ turbulence model. J. Wind Eng. Ind. Aerodyn. 46–47, 145–153.
Roache, P.J., 1994. Perspective: a method for uniform reporting of grid refinement studies. J. Fluids Eng. 116, 405.
Roache, P.J., 1997. Quantification of uncertainty in computational fluid dynamics. Annu. Rev. Fluid. Mech 29, 123–60.
Sato, T., Uematsu, T., Nakata, T., Kaneda, Y., 1993. Three-dimensional numerical simulation of snowdrift. J. Wind Eng. Ind. Aerodyn. 46 & 47, 741–746.
Schmidt, R.A., 1986. Transport rate of drifting snow and the mean wind speed profile. Boundary-Layer Meteorol. 34, 411–414.
Shih, T.-H., Liou, W.W., Shabbir, A., Yang, Z., Zhu, J., 1995. A new k-ϵ eddy viscosity model for high reynolds number turbulent flows - model development and validation. Comput. Fluids 24, 227–238.
Smedley, D.J., Kwok, K.C.S., Kim, D.H., 1993. Snowdrifting simulation around Davis Station workshop, Antarctica. J. Wind Eng. Ind. Aerodyn. 50, 153–162.
Sundsbø, P., 1998. Numerical simulations of wind deflection fins to control snow accumulation in building steps. J. Wind Eng. Ind. Aerodyn. 74, 543–552.
Tabler, R.D., 2003. Controlling blowing and drifting snow with snow fences and road design, NCHRP Project 20-7(147), National Cooperative Highway Research Program Transportation Research Board of the National Academies.
Takeuchi, M., 1980. Vertical profile and horizontal increase of drift-snow transport. J. Glaciol. 26, 481–492.
Thiis, T.K., Gjessing, Y., 1999. Large-scale measurements of snowdrifts around flat-roofed and single-pitch-roofed buildings. Cold Reg. Sci. Technol. 30, 175–181.
Thiis, T.K., Potac, J., Ramberg, J.F., 2009. 3D numerical simulations and full scale measurements of snow depositions on a curved roof, in: The 5th European & African Conference on Wind Engineering. Florence,Italy.
Thiis, T.K., O'Rourke, M., 2015. Model for snow loading on gable roofs. J. Struct. Eng. 141, 4015051.

Thiis, T.K., Ferreira, A.D., 2015. Sheltering effect and snow deposition in arrays of vertical pillars. Environ. Fluid Mech. 15, 27–39.
Tominaga, Y., Mochida, A., 1999. CFD prediction of flowfield and snowdrift around a building complex in a snowy region. J. Wind Eng. Ind. Aerodyn. 81, 273–282.
Tominaga, Y., Mochida, A., Yoshino, H., Shida, T., Okaze, T., 2006. CFD Prediction of Snowdrift around a Cubic Building Model, in: The Fifth International Symposium on Computational Wind Engineering（CWE2006). pp. 941–944.
Tominaga, Y., Stathopoulos, T., 2007. Turbulent Schmidt numbers for CFD analysis with various types of flowfield. Atmos. Environ. 41, 8091–8099.
Tominaga, Y., Mochida, A., Yoshie, R., Kataoka, H., Nozu, T., Yoshikawa, M., Shirasawa, T., 2008. AIJ guidelines for practical applications of CFD to pedestrian wind environment around buildings. J. Wind Eng. Ind. Aerodyn. 96, 1749–1761.
Tominaga, Y., Okaze, T., Mochida, A., 2011a. CFD modeling of snowdrift around a building: An overview of models and evaluation of a new approach. Build. Environ. 46, 899–910.
Tominaga, Y., Mochida, A., Okaze, T., Sato, T., Nemoto, M., Motoyoshi, H., Nakai, S., Tsutsumi, T., Otsuki, M., Uamatsu, T., Yoshino, H., 2011b. Development of a system for predicting snow distribution in built-up environments: Combining a mesoscale meteorological model and a CFD model. J. Wind Eng. Ind. Aerodyn. 99, 460–468.
Tominaga, Y., 2017. Computational fluid dynamics simulation of snowdrift around buildings: Past achievements and future perspectives. Cold Reg. Sci. Technol. DOI: https://doi.org/10.1016/j.coldregions.2017.05.004
Tsuchiya, M., Tomabechi, T., Hongo, T., Ueda, H., 2002. Wind effects on snowdrift on stepped flat roofs. J. Wind Eng. Ind. Aerodyn. 90, 1881–1892.
Uematsu, T., Nakata, T., Takeuchi, K., Arisawa, Y., Kaneda, Y., 1991. Three-dimensional numerical simulation of snowdrift. Cold Reg. Sci. Technol. 20, 65–73.
van Hooff, T., Blocken, B., 2010. Coupled urban wind flow and indoor natural ventilation modelling on a high-resolution grid: A case study for the Amsterdam ArenA stadium. Environ. Model. Softw. 25, 51–65.
van Hooff, T., Blocken, B., Tominaga, Y., 2017. On the accuracy of CFD simulations of cross-ventilation flows for a generic isolated building: Comparison of RANS, LES and experiments. Build. Environ. 114, 148–165.
Wilcox, D.C., 1998. Turbulence Modelling for CFD, DCW Industries, Inc. La Canada, California.
Yakhot, V., Orszag, S. a., Thangam, S., Gatski, T.B., Speziale, C.G., 1992. Development of turbulence models for shear flows by a double expansion technique. Phys. Fluids 4, 1510–1520.
Zallen, R., 1988. Roof collapse under snowdrift loading and snowdrift design criteria. J. Perform. Constr. Facil. 2, 80–98.
Zhou, X., Hu, J., Gu, M., 2014. Wind tunnel test of snow loads on a stepped flat roof using different granular materials. Nat. Hazards 74, 1629–1648.
Zhou, X., Kang, L., Yuan, X., Gu, M., 2016a. Wind tunnel test of snow redistribution on flat roofs. Cold Reg. Sci. Technol. 127, 49–56.
Zhou, X., Qiang, S., Peng, Y., Gu, M., 2016b. Wind tunnel test on responses of a lightweight roof structure under joint action of wind and snow loads. Cold Reg. Sci. Technol. 132, 19–32.
Zhou, X., Kang, L., Gu, M., Qiu, L., Hu, J., 2016c. Numerical simulation and wind tunnel test for redistribution of snow on a flat roof. J. Wind Eng. Ind. Aerodyn. 153, 92–105.

Tables and figures

Table 1 Physical and computational parameters used by previous researchers in the simulation of snow drift for application purposes.

	Research object	w_f [m/s]	Sc_t [-]	u_{*t} [m/s]	ρ_s [kg/m^3]
Uematsu et al. (1991)	Snowdrift around snow fences, a wind scoop and a hill	0.50	1.0	0.20	-
Naaim et al. (1998)	Snowdrift around a snow fence	0.30 0.45	-	0.36	-
Sundsbø (1998)	Snowdrift around a building	$w_{sus}=0.3\frac{\mu}{\mu+\mu_t}$ $w_{sal}=c_f(1-f)f\frac{\nabla p}{\rho_m}$	1.0	0.25	700
Tominaga and Mochida (1999)	Snowdrift around a building	0.50	1.0	-	-
Alhajraf (2004)	Snowdrift around a snow fence	-	-	0.22	-
Beyers et al. (2004)	Snowdrift around a cube	0.50	1.0	0.28	-
Tominaga et al. (2006)	Snowdrift around a cube	1.00	1.0	0.15	150
Beyers and Waechter (2008)	Snowdrift around complex structures	0.45	-	0.28	560
Thiis et al. (2009)	Snow depositions on a curved roof	0.50	-	0.25	50 150
Potac and Thiis (2011)	Snowdrift on a gable roof	0.50	-	0.29	150
Tominaga et al. (2011a)	Snowdrift around a building	0.50	1.0	0.20	100
Tominaga et al. (2011b)	Snowdrift around a cube	0.20	1.0	0.15 0.21	150

Zhou et al. (2016c)	Snow transport on a flat roof	0.20	1.0	0.20	150

Sundsbø (1998) used two different falling velocities in the simulation, w_{sal} for snow saltation and w_{sus} for snow suspension. The idea behind the equation for w_{sus} is that laminar flow conditions give the highest vertical falling velocity, which can be regarded as a terminal bulk velocity for suspended snow particles, of all sizes (Sundsbø, 1998). In the above table, μ and μ_t are laminar and turbulent dynamic viscosity, respectively. ∇p is the pressure gradient and c_f is the reciprocal drag coefficient between air and snow. f is the snow volume fraction. The mixture density ρ_m is obtained from the snow density ρ_s and the air density ρ_{air}, where $\rho_m = f\rho_s + (1-f)\rho_{air}$.

Table 2 Properties of snow and/or falling snow as derived from field measurements.

	w_f [m/s]	Sc_t [-]	u_{*t} or U_t [m/s]	ρ_s [kg/m^3]	d_p [mm]	Description
Nakaya and Terada (1935)	0.07-0.50 0.32-0.78 0.90-1.00	-	-	-	0.2-5.0 1.4-5.0 1.2-3.8	Plane dendritic snow crystals Spatial dendritic snow crystals Rimed snow crystals
Kajikawa (1975)	0.13-0.62 0.20-0.70 0.20-1.20	-	-	-	0.4-4.8 1.1-4.9 0.7-5.0	Plane dendritic snow crystals Spatial dendritic snow crystals Rimed snow crystals
Gray and Male (1981)	-	-	0.15 or 4.0 0.25 or 5.5 0.40 or 8.5	-	-	Loose fresh, -2.5 °C, H_{ref} = 1 m Newly fallen, 0 °C, H_{ref} = 1 m Slightly aged, 0 °C, H_{ref} = 1 m
Schmidt (1986)	-	-	0.20-0.51	-	0.14-0.22	After precipitation
Pomeroy and Gray (1990)		-	0.20-0.33	-	0.08-0.16	-
Beyers and Harms (2003)	-	-	8	450-550	-	Old compacted snow, H_{ref} = 10 m
Doorschot et al. (2004)	-	-	0.21-0.69	120-354	0.27-0.68	-
Cierco et al. (2007)	-	-	-	250 270 320 78	<0.5 <0.5 <0.5 Unknown	Small rounded grains, -7 °C Small rounded grains, -16 °C Small rounded grains, -8 °C New snow, -19 °C
Naaim-Bouvet et al. (2013)	-	0.5-1.3	-	-	0.095-0.105 0.105-0.125 0.175-0.220	Height: 3.34m-3.48m Height: 1.13m-1.28m Height: 0.13m-0.27m

Table 3 Computational settings for the reference case.

	Computational settings
Computational domain	3000 m (L) × 10 m (H)
Grid discretization	Stretching ratio: 1.10 (length), 1.05 (height). Minimum grid size: 0.30 m (length), 0.008 m (height). Total cell count: 211,000.
Inlet boundary	Velocity inlet: Eqs. (13)-(16).
Outlet boundary	Zero static gauge pressure.
Ground boundary	No-slip wall with standard wall functions (Launder and Spalding, 1974); roughness modification (Cebeci and Bradshaw, 1977); roughness relationship k_S-z_0 (Blocken et al., 2007). k_S = 0.0029 m, C_S = 2.0.
Upper boundary	Symmetry
Discretization scheme for convection and viscous terms	Second-order upwind
Turbulence model	Realizable k-ε model (Shih et al., 1995)
Convergence criteria	All the scaled residuals level off and reach a minimum of 10^{-11} for continuity, 10^{-14} for x velocity, y velocity, k and ε, and 10^{-15} for snow.

Table 4 Physical and computational parameters for the reference case.

w_f [m/s]	Sc_t [-]	u_{*t} [m/s]	u_* [m/s]
0.48 ($z \leq 0.1$ m) 0.24 ($z > 0.1$ m)	1.0	0.27	0.31

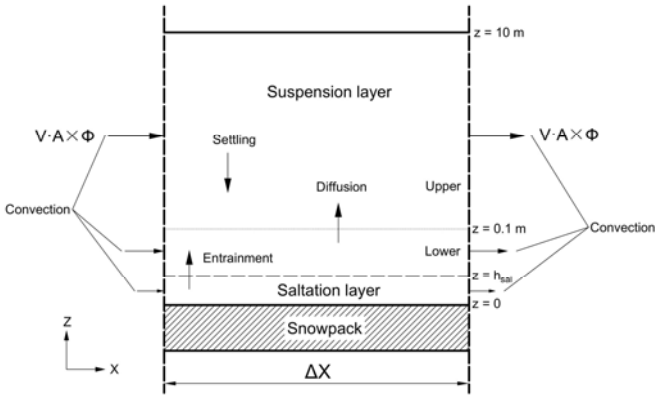

Fig. 1. Control volume and simulation scheme.

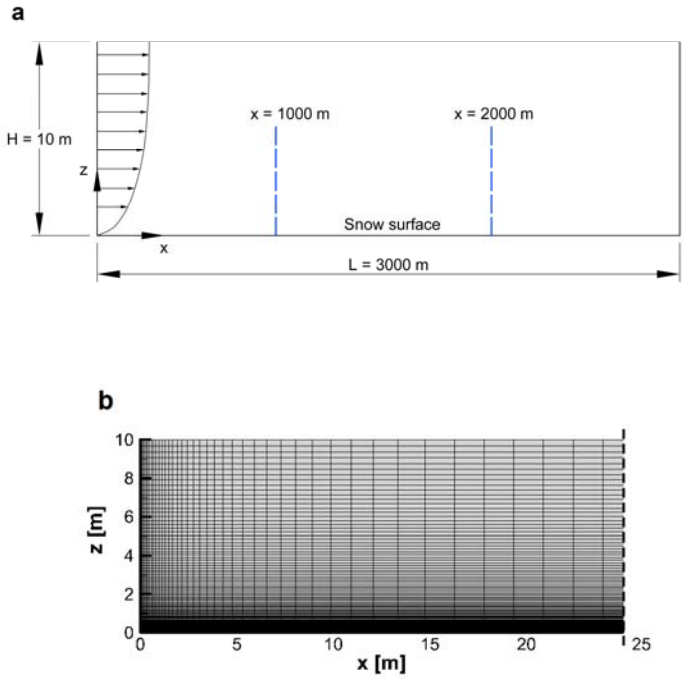

Fig. 2. (a) Computational domain (not to scale). (b) Part of computational grid with 211,000 cells.

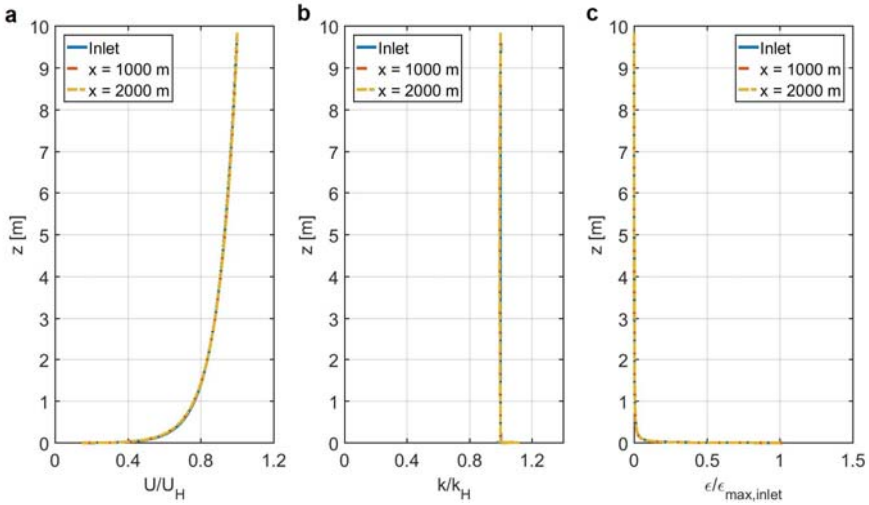

Fig. 3. Dimensionless mean wind speed and turbulence profiles at three separate locations (H = 10 m, realizable *k*-*ε* model). (a) Dimensionless mean wind speed; (b) dimensionless turbulent kinetic energy; (c) dimensionless turbulence dissipation rate.

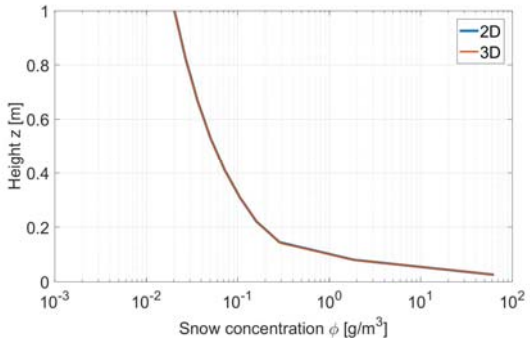

Fig. 4. Comparison of snow concentrations (ϕ) from 3D simulation and 2D simulation.

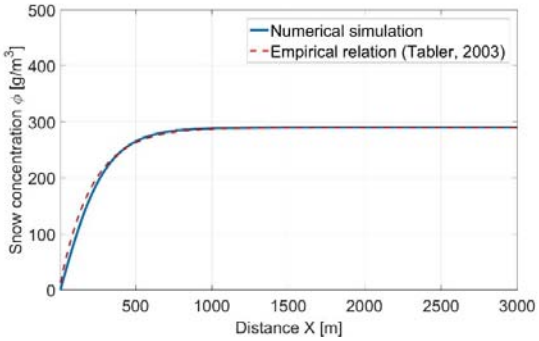

Fig. 5. Snow concentration (ϕ) near the snow surface.

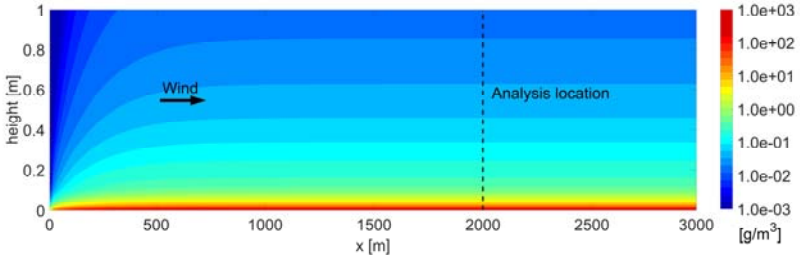

Fig. 6. Spatial distribution of snow concentration.

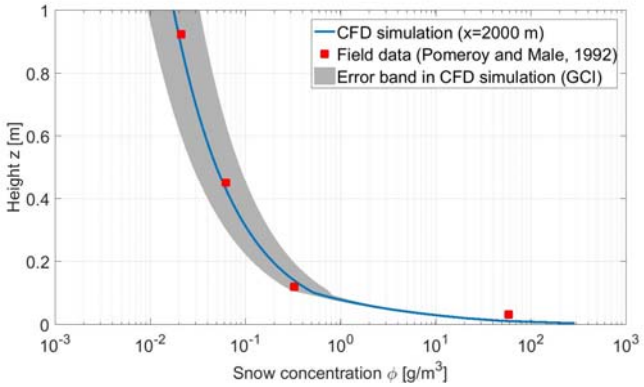

Fig. 7. Vertical distribution of snow concentration during snow transport.

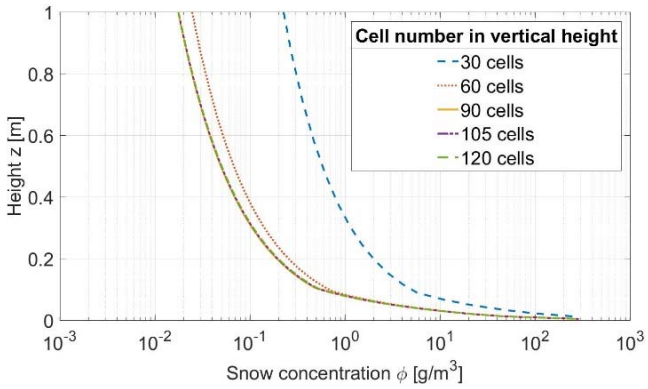

Fig. 8. Impact of grid resolution on the snow concentrations (ϕ) predicted by CFD.

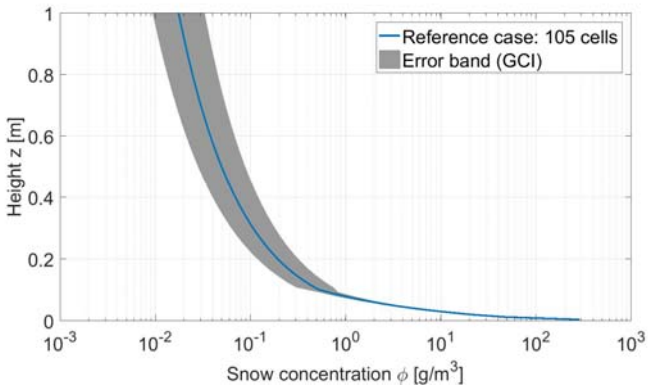

Fig. 9. Grid-convergence index (GCI) of snow concentration for the reference grid.

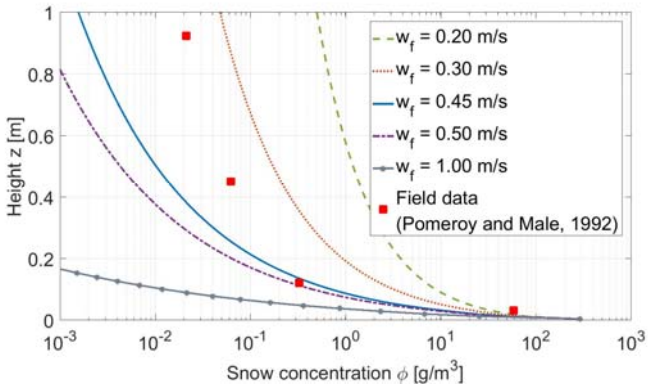

Fig. 10 Impact of falling velocity (w_f) on the vertical distribution of drifting snow (Sc_t = 1.0).

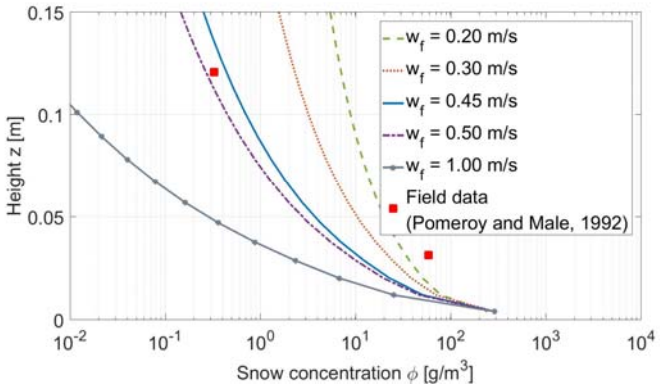

Fig. 11 Impact of falling velocity (w_f) on the vertical distribution of drifting snow in the lower part of the domain

(Sc_t = 1.0, z $\leq$ 0.15 m).

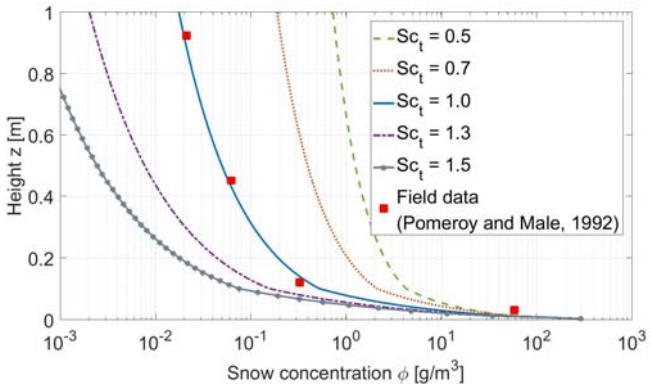

Fig. 12. Impact of turbulent Schmidt number (Sc_t) on the vertical distribution of drifting snow.

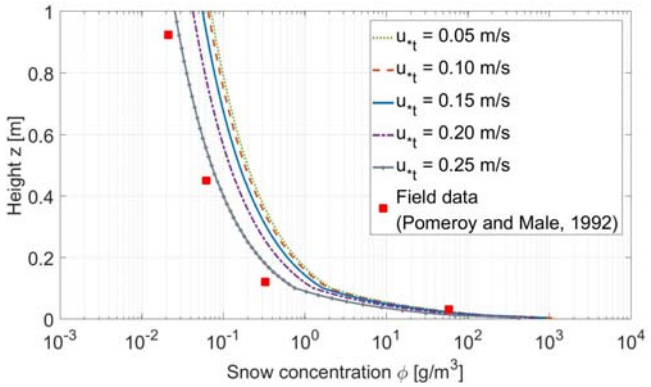

Fig. 13. Impact of threshold friction velocity (u_{*t}) on the vertical distribution of drifting snow**.**

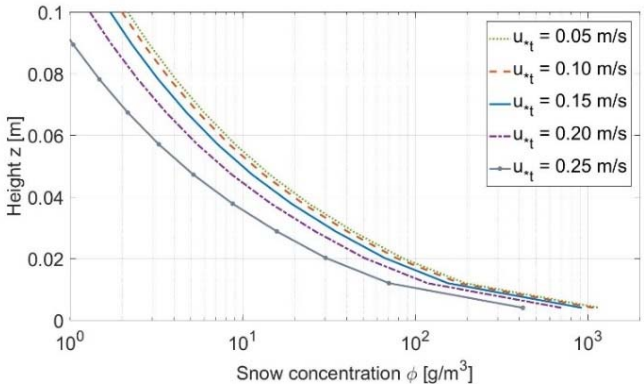

Fig. 14. Impact of threshold friction velocity (u_{*t}) on the vertical distribution of drifting snow in the lower part
($z \leq 0.10$ m).

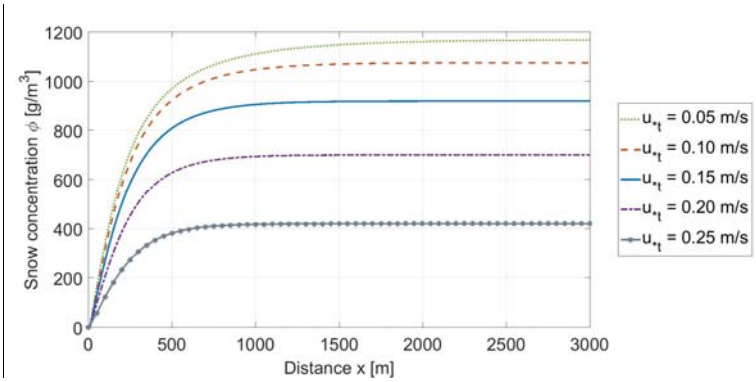

Fig. 15. Impact of threshold velocity (u_{*t}) on the distribution of snow concentration near the ground.

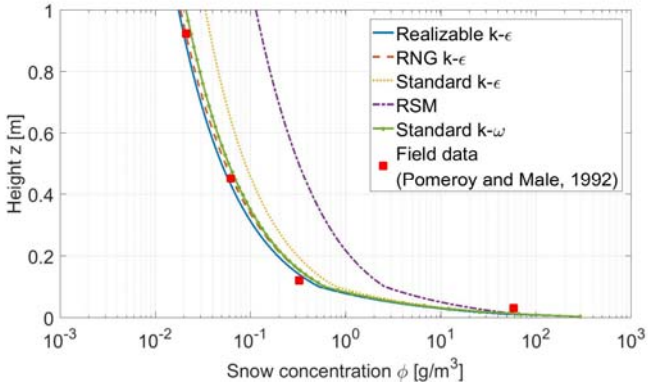

Fig. 16. Impact of turbulence model on the vertical distribution of drifting snow.

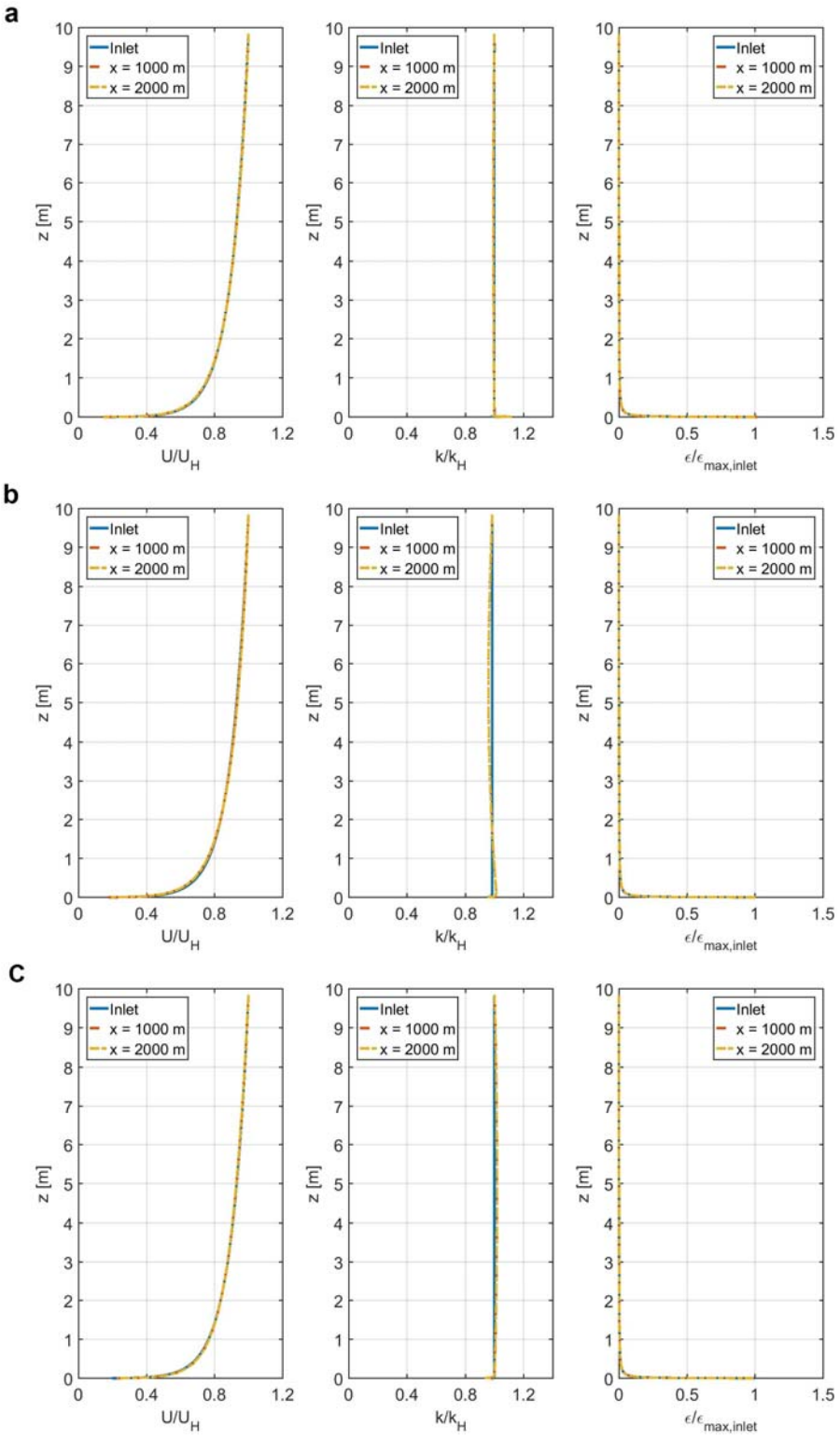
a
b
c
Inlet
x = 1000 m
x = 2000 m
z [m]
U/U_H
k/k_H
ε/ε_max,inlet

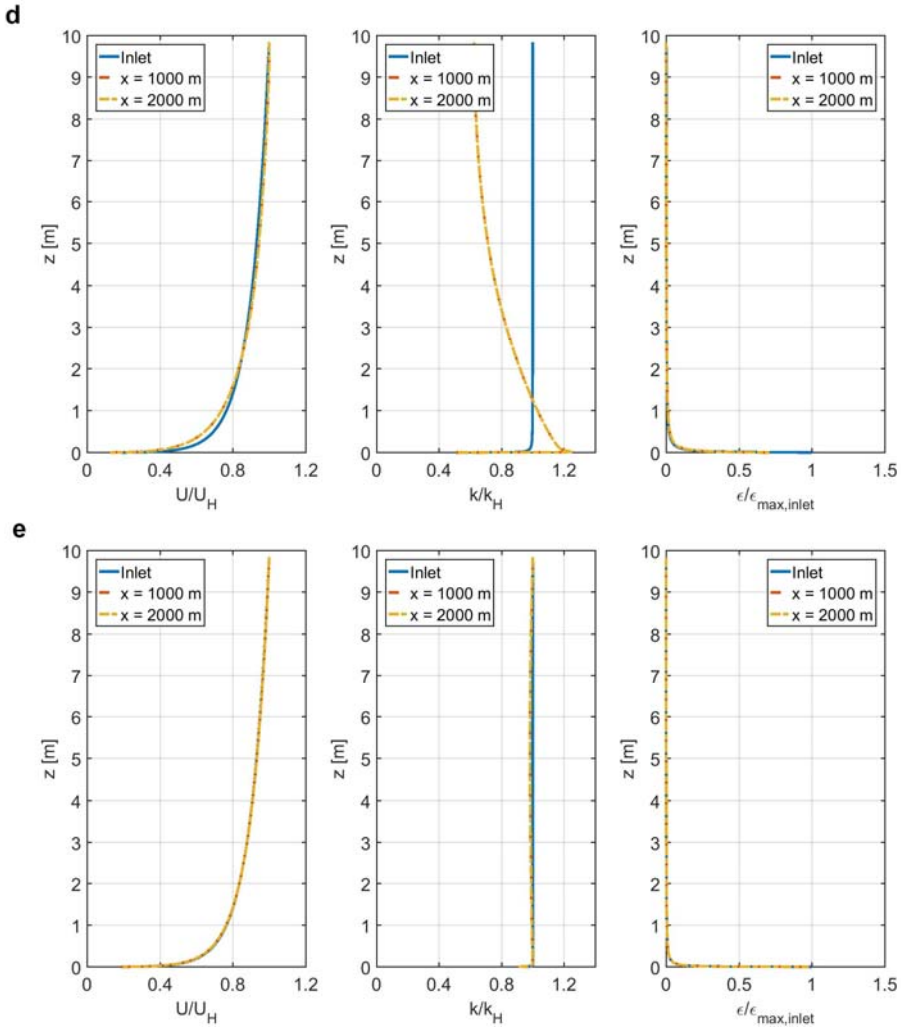

Fig. 17. Vertical profiles of dimensionless mean wind speed, dimensionless turbulent kinetic energy and dimensionless turbulence dissipation rate for different turbulence models. (a) Realizable k-ε model; (b) RNG k-ε model; (c) standard k-ε model; (d) Reynolds stress model; (e) standard k-ω model.